

Terahertz resonant emission by optically excited infrared-active shear phonons in $\text{KY}(\text{MoO}_4)_2$

D. Kamenskyi,^{1,2,3} K. Vasin,³ L. Prodan,³ K. Kutko,⁴ V. Khrustalyov,⁴ S. G. Pavlov,¹ and H.-W. Hübbers^{1,2}

¹*Institute of Optical Sensor Systems, German Aerospace Center (DLR), Rutherfordstr. 2, 12489 Berlin, Germany*

²*Department of Physics, Humboldt-Universität zu Berlin, Newtonstr. 15, 12489 Berlin, Germany*

³*Experimental Physics V, Center for Electronic Correlations and Magnetism,*

Institute of Physics, University of Augsburg, 86159 Augsburg, Germany

⁴*B. Verkin Institute for Low Temperature Physics and Engineering of the National Academy of Sciences of Ukraine, Nauky Avenue 47, 61103 Kharkiv, Ukraine*

Generation of the monochromatic electromagnetic radiation in the terahertz (THz) range of frequencies for many decades remains a challenging task. Here we demonstrate the emission of monochromatic sub-THz radiation by coherent optical phonons in dielectric material $\text{KY}(\text{MoO}_4)_2$. The layered crystal structure of $\text{KY}(\text{MoO}_4)_2$ leads to infrared-active shear lattice vibrations with energies below 3.7 meV, which corresponds to the frequencies low than 900 GHz where solid-state compounds based monochromatic radiation sources are rare. Coherent infrared-active optical phonons are excited by broadband THz pulses lasting for tens of picoseconds and re-emit narrow-band sub-THz radiation pulses with a decay time of 33 picoseconds, which is exceptionally long for the oscillators with frequencies below 1 THz. Such a long coherent emission allows for the detection of more than 50 periods of radiation with frequencies of 568 and 860 GHz. The remarkably long decay time together with the chemical stability of the employed materials suggest a variety of possible applications in THz laser technology.

Last decades significant achievement in the Time-Domain Terahertz Spectroscopy (THz-TDS) boost interest to THz research and its application [1]. THz-TDS method is based on electromagnetic transients optoelectronically generated by ultrashort, usually femtosecond, laser pulses. The single-cycle bursts of electromagnetic radiation typically have duration about 1 ps with the spectral density enhanced between 100 GHz and 5 THz [2]. It is well known that a time-varying electric dipole moment emits electromagnetic wave on the oscillation frequency of the dipole [2]. For the first time, the photo-Dember effect of electromagnetic wave re-emission by coherent phonons in the THz range of frequencies has been reported in tellurium single-crystal [3]. Recently, it was also reported in hybrid perovskites [4], charge-density wave system $\text{K}_{0.3}\text{MoO}_3$ [5], and topological material TaAs where it offers opportunities for THz emission with polarization control [6]. The recent overview of the THz re-emission by optically pumped solids is given elsewhere [7]. Generally, the photo-Dember THz re-emission is broadband with the typical spectrum width above 100 GHz.

Despite the achieved progress, the generation of the monochromatic THz radiation, remains a challenging task. However for such applications as a THz imaging [8], THz-driven particle acceleration [9] or ultrafast phase-changes [10], narrow-band THz pulses is crucial. Lithium niobate [11] as well as other materials (semiconductors [12] and organic crystals [13]) have been reported as perspective materials for generating high-energy narrow-band THz pulses with the typical bandwidth of about 1%. Here we report observation of a narrow-band (full width on half maximum $\Delta\nu < 4$ GHz or 0.5%) re-emission of

THz electromagnetic pulses by $\text{KY}(\text{MoO}_4)_2$ single crystals pumped by a broadband THz excitation pulse in a conventional THz-TDS setup. $\text{KY}(\text{MoO}_4)_2$ is a solid dielectric material whose dipole-active shear lattice vibrations lie in THz frequencies range. The observed length of the re-emitted pulses of quasi-monochromatic electromagnetic radiation is over a hundred of picoseconds (tens of optical cycles), that is longer than the photon transient time in the used crystals. We explain this emission as resonant re-emitted light due to photo-excitation of infrared-active vibrational shear modes in $\text{KY}(\text{MoO}_4)_2$.

$\text{KY}(\text{MoO}_4)_2$ belongs to a series of molybdate compounds with general chemical formula $M\text{R}(\text{MoO}_4)_2$, where M^+ is an alkali metal ion and R^{3+} is a rare-earth or Y^{3+} ion. These are optically transparent dielectric compounds with a high permittivity ($\epsilon > 15$) and orthorhombic structure $Pbcn$ (D_{2h}^{14}) which is formed by $[\text{R}(\text{MoO}_4)_2]^-$ layers in ac plane coupled via M^+ ions along the b direction (see crystallographic structure in Figure 1) [14]. The detailed description of the synthesis is given in Ref. [15]. $\text{KY}(\text{MoO}_4)_2$ single crystals used for this study have been grown in the Institute for Low Temperature Physics (Kharkiv, Ukraine). The compositional analysis of the crystals was done using scanning electron microscopy in combination with the energy-dispersive X-ray spectroscopy and elemental mapping.

In recent years rare-earth based molybdates attract attention due to a giant rotational magnetocaloric [16] and massive magnetostriction [17] effects induced by large anisotropy of the R^{3+} ion. Here we exploit a large anisotropy of the crystal lattice of $\text{KY}(\text{MoO}_4)_2$ for the

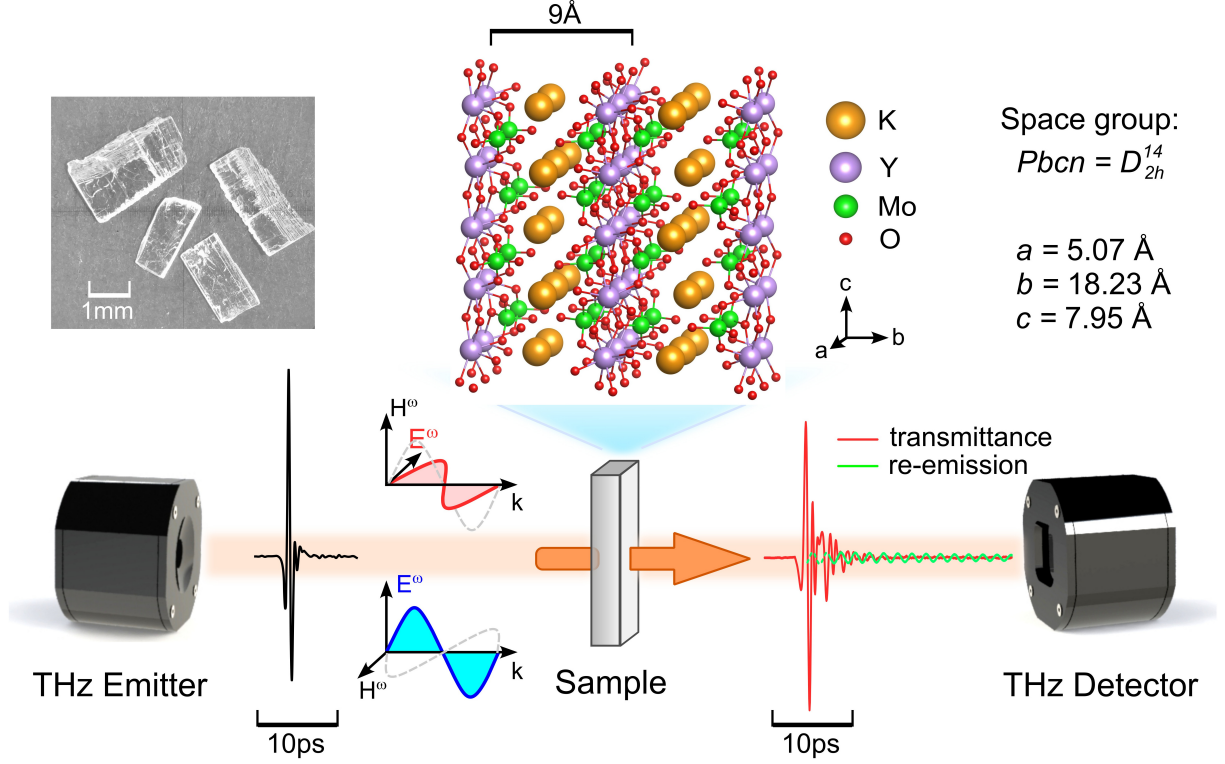


FIG. 1. Top. A photograph and the crystallographic structure of KY(MoO₄)₂ single crystal. Bottom. A schematic representation of THz-TDS setup: black trace shows THz waveform of incident light (from THz emitter). Red and green curves show the components of the beam which enters the detector. The cryogenic part of the setup is omitted for clarity. E^ω stands for the electric field magnitude of electromagnetic wave.

emission of THz radiation. In our experiments we used the plate-shaped single crystals (Figure 1 left) with the crystallographic b axis perpendicular to the plates. Due to a weak bonding between $[R(\text{MoO}_4)_2]^-$ layers, single crystals cleave along ac plane.

THz-TDS spectra were measured using a table-top time-domain terahertz platform TeraFlash (TOPTICA Photonics AG). In these experiments, the radiation was propagating along the b -axis of the crystal, and linearly polarised along the a and c .

Figure 1 shows a sketch of the experimental setup, image of samples and the crystallographic structure of KY(MoO₄)₂ crystal. The specimen was mounted to a brass holder with 4 mm aperture inside the Spectromag cryostat (Oxford Instruments) (which is omitted in the Figure 1 for clarity) with insert which allows temperature variation between 3 and 300 K. The black curve shown before the sample in Figure 1 represents a temporal profile of electric field during the THz pulse measured when the radiation passed the empty aperture (excitation pulse), and curves after the sample show the profile measured when the pulse passed the sample. The pulse after the sample contains contributions of the distorted initial TDS pulse (red curve) and the radiation re-emitted by the crystal (green curve), further we discuss the micro-

scopic mechanism of this re-emission. The square of the ratio of the Fourier transforms of the measured transients returns the sample's transmittance spectrum (transmitted energy). Taking this ratio as a transmittance, we assume that the sample does not affect significantly the efficiency of the light collection by the detector.

Figure 2 top displays the transmittance spectra of 80 μm thick KY(MoO₄)₂ single crystal at frequencies between 0.3 and 1.5 THz measured at 4 K. Red and blue curves correspond to the THz wave polarised along a and c crystallographic axes respectively ($E^\omega \parallel a$ and $E^\omega \parallel c$, where E^ω is the electric field magnitude of the electromagnetic wave). Sharp peaks S_a and S_c at 568 and 860 GHz (phonon energy equivalents are 2.35 and 3.56 meV) respectively, are due to dipole active shear lattice vibrations, when $[\text{Y}(\text{MoO}_4)_2]^-$ and K^+ layers move as a whole in ac plane as has been shown earlier [14]. A large mass of $[\text{Y}(\text{MoO}_4)_2]^-$ layers together with weak bonding between them causes the frequency of these vibrations are below 1 THz, while typical optical phonons in solids have frequencies above 3 THz [18]. Remarkably, the S_c absorption is about 10 times stronger than S_a . This makes the sample opaque for $E^\omega \parallel c$ radiation with frequencies in a vicinity of S_c peak (Figure 2), and cause a peculiarity in the re-emission spectrum of S_c phonon which we are

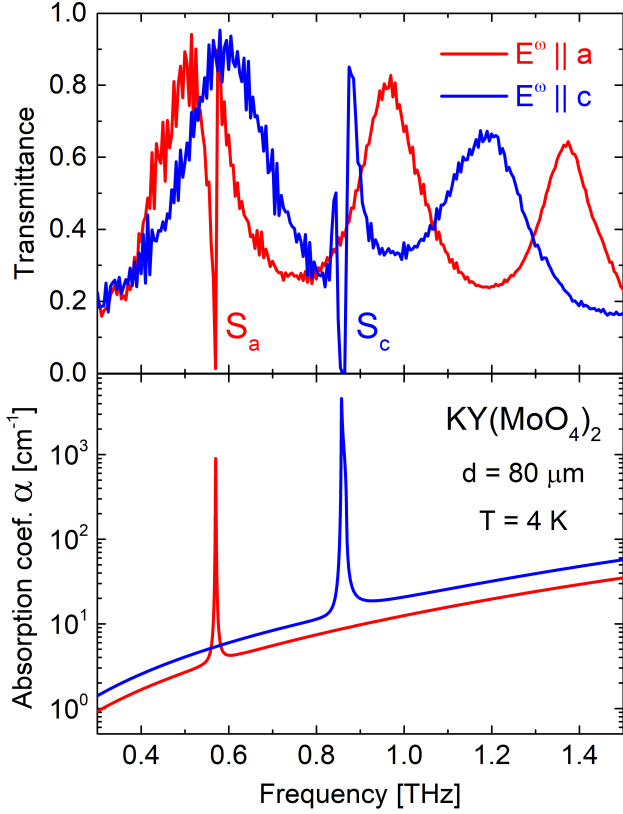


FIG. 2. Top. Transmittance spectra of 80 μm thick KY(MoO₄)₂ sample for $E^\omega \parallel a$ (red) and $E^\omega \parallel c$ (blue) polarisations. Multiple reflections within the plane-parallel sample result in Fabry-Perot type modulation of spectra. Bottom. Frequency dependence of the absorption coefficient $\alpha(\omega)$ obtained using REFFIT script [19].

going to discuss further in the text.

Multiple reflections of the radiation within the plane-parallel sample result in interference fringes of the transmission spectra (Figure 2 top). The periodicity of the fringes determined by the thickness of the crystal, d , and the refractive index, n , of the sample. We used REFFIT script [19] to determine the complex dielectric function of the material, $\hat{\epsilon}(\omega) = \epsilon_1 - i\epsilon_2$, and, consequently, frequency dependence of the refractive index, n , the optical extinction coefficient, κ , and the absorption coefficient $\alpha(\omega) = 2\kappa\omega/c_0 = 2\omega/c_0 \sqrt{1/2 \cdot (\epsilon_1^2 + \epsilon_2^2)^{1/2} - \epsilon_1/2}$ (Figure 2 bottom) where c_0 is the speed of light in vacuum. According to the Beer-Lambert law, $I(d) = I_0 e^{-\alpha \cdot d}$ (d is the sample thickness), $1/\alpha$ corresponds to the sample thickness when the light intensity, I , decays in e times.

Extremely low width of the peaks (for $E^\omega \parallel a$ it is below reliable resolution limit of 5 GHz) reflects exceptionally large lifetime of such a dipole. To the best of our knowledge, these are the sharpest phonon peaks ever

observed below 1 THz. The lifetime could be estimated as $\tau = (\pi\Delta\nu)^{-1} \approx 100$ ps [20, 21] (where $\Delta\nu$ is the full width at half maximum of S_a mode in the $\alpha(\omega)$ spectrum, Figure 2 bottom). Thus, τ of S_a phonon is an order of magnitude exceeds usual phonons lifetime (typically 1 – 10 ps) and the duration of the excitation THz pulse in our setup (~ 5 ps). For the S_c phonon such estimation is not possible because of the strong absorption in a vicinity of S_c and the transmitted signal between 857 and 863 GHz is below the noise level of the detector and the peak is distorted (later in the text we call such distortion of the peak *saturation*).

Figure 3a shows the electric field waveform of the broadband THz pulse which reaches the detector via an empty aperture. This signal decays within 4-5 ps and, obviously, corresponds to the pulse before it passed the sample (losses in optical elements are assumed to be the same for the beams passing the cryostat with and without sample). The waveforms which passed 80 μm thick sample (Figures 3b, 3c for $E^\omega \parallel a$ and $E^\omega \parallel c$ respectively) exhibit scintillating signals on phonon frequencies for tens of picoseconds. Note, the transmitted signal is also delayed by 1 ps due to a large refractive index of KY(MoO₄)₂, $nd/c_0 \sim 1$ ps ($n \approx 4$ below 1 THz). For $E^\omega \parallel a$, the waveform shows oscillations with S_a phonon frequency with the decay an order of magnitude longer than the initial pulse (highlighted by the yellow background in 3b and zoomed in Figure 3d). This long extended emission tail is a manifestation of the electromagnetic wave re-emission by coherent phonons in KY(MoO₄)₂. Dashed line in Figure 3d shows the exponential decay of radiation intensity fitted by $\exp(-t/\tau_e)$ where $\tau_e = 33$ ps is the decay time. Such a long decay and significant intensity of the signal allow the observation of tens of optical periods of monochromatic electromagnetic wave. Figure 3f shows the Fourier transformation (FFT) of the signal from Figure 3d. As one can see, 10 ps after the excitation pulse, the electromagnetic radiation with $E^\omega \parallel a$ behind the KY(MoO₄)₂ sample is practically monochromatic light with the frequency exactly the same to the absorption frequency of S_a phonon. In contrast to $E^\omega \parallel a$, the waveform for $E^\omega \parallel c$ (Figure 3c) after main peak exhibits a beating of two frequencies (Figure 3e) around the resonance frequency of S_c phonon (see FFT in Figure 3g). Later we show that this beating is a manifestation of the saturation observed in the transmittance spectra (Figure 2 top, blue curve). The strong intensity of S_c phonon prohibits the propagation of resonance frequency in material while the lattice vibrations on frequency near by the resonance efficiently re-emit the electromagnetic radiation.

In order to confirm that splitting of the re-emission peak for $E^\omega \parallel c$ is caused by the strong intensity of S_c phonon, we study the temperature transformation of the

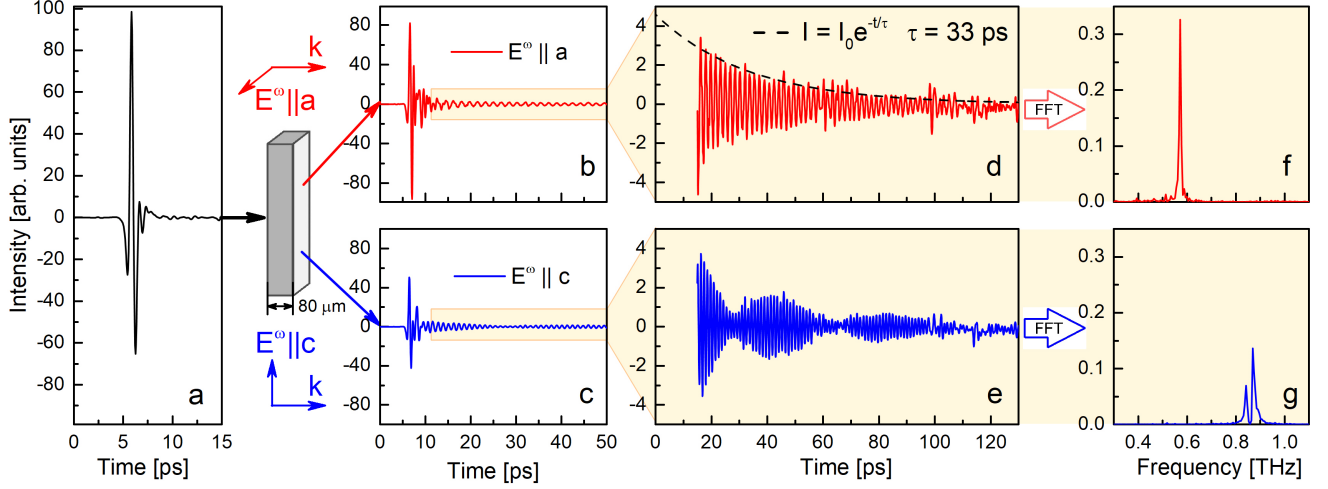


FIG. 3. (a) The electric field waveform of the THz pulse before the sample. (b, c) Waveforms of the THz pulse passed the sample for polarisations along a (red) and c (blue) axes. (d, e) Zoomed waveforms for the a (red) and c (blue) polarisations 10 ps after the start of the pulse. (f, g). Squared FFT of the waveforms shown in 3d and 3e, respectively.

spectra. Figure 4 displays the evolution of transmittance (left) and re-emission (right) spectra of $\text{KY}(\text{MoO}_4)_2$ for $E^\omega \parallel c$ upon a cooling. The re-emission spectra were obtained in the same manner as in Figures 3f and 3g. As temperature decreases the phonon peak S_c gets narrow and grows in amplitude which leads to the development of the re-emission peak splitting simultaneously with saturation of the absorption peaks. As one can see Figure 4, the re-emission spectrum at room temperature (270 K) have monochromatic lorentzian shape. Upon a cooling the frequencies where the absorption is strongest are missing in re-emission spectrum which leads to a spectral dip in the emission peak. We note, that remarkably strong re-emission at room temperature significantly enlarges the application perspectives.

Similar peak splitting, we observe in a thickness dependence of the re-emission spectrum (Figure 5 ($E^\omega \parallel a$)). One can see that maximal re-emission intensity of the 65 μm thick sample is significantly smaller than for 80 μm one. These thicknesses is not far from the value of $1/\alpha_a \approx 10$ μm at S_a frequency. When the sample thickness grows further, the intensity of the re-emission decays, because obviously the radiation spend more time inside the material and the energy dissipate into other optical and acoustic phonons. When $d \gg 1/\alpha$ by an order of magnitude the re-emission intensity on the central frequency decays, while on frequencies near by the resonance the re-emission remains efficient as it has been described above for the $E^\omega \parallel c$ polarisation. This leads to the beating in the time-domain spectra (Figure 3e) and to the spectral dip in the re-emission peak (Figure 3g).

Beating shapes of TDS transients propagating through the media with strong, spectrally narrow absorption peaks have attracted attention of many theoretical groups in past. Different phenomena, such as so-called Sommerfield-Brillouin forerunners [22], dynamical beats, and optical precursors generated by the incident step-modulated pulses, were utilized to explain similar experimental observations. We point a comprehensive work by Bruno and Bernard [23] focused on the response function of the dielectric medium with a single absorption line. It outlines the conditions for observing dynamical beats: $1 \ll \alpha d \ll \nu_0/\Delta\nu$, where ν_0 represents the central frequency of the absorption line, and d stands for the thickness of the slab. In our case, for an 80 μm sample at 4 K, this results are $1 \ll 7 \ll 475$ for the S_a phonon and $1 \ll 37 \ll 329$ for the S_c phonon. Thus, for both polarisation the condition is met. However, detailed discussion of the microscopic mechanism of the beating formation would require significantly higher spectral resolution, which is not feasible for the current TDS spectroscopy and goes beyond the scope of this study, where we focus on the optimal conditions for the monochromatic THz re-emission.

Thus, in $\text{KY}(\text{MoO}_4)_2$ the radiation energy absorbed by the S_a phonon during the initial THz excitation pulse (~ 5 ps) is not converted to the sample heating via phonon-phonon interactions (which is a common relaxation channel for the lattice excitations in solids) due to limited coupling of the share vibrations to other phonons. Instead, the most of these energy is re-emitted via mechanism of classical time-varied dipole by the coherent dipole

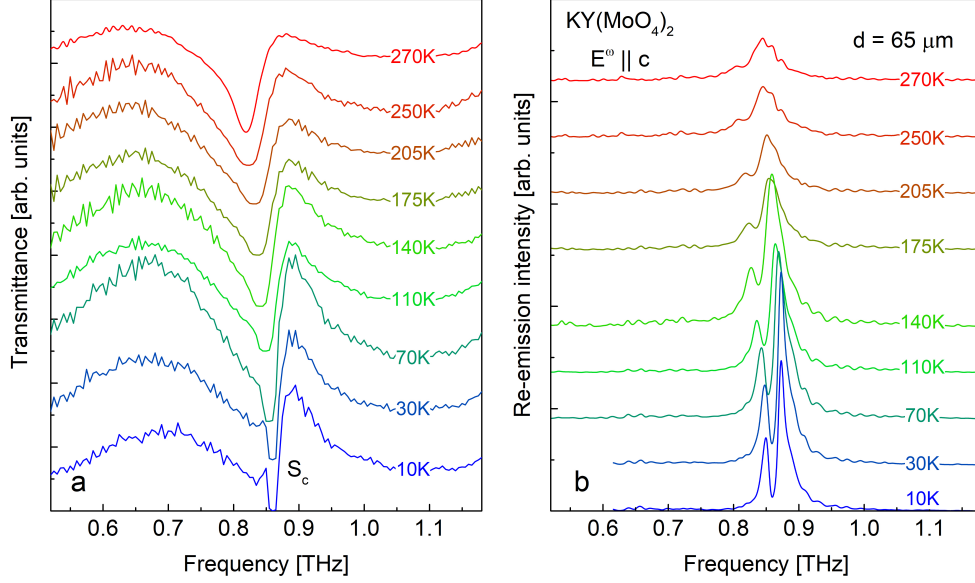


FIG. 4. Temperature evolution of the transmittance (a) and re-emission (b) spectra for the $65\mu\text{m}$ thick $\text{KY}(\text{MoO}_4)_2$ sample at $E^\omega \parallel c$. Here, we call the FTT as “re-emission” after 10 ps delay from the pump pulse front.

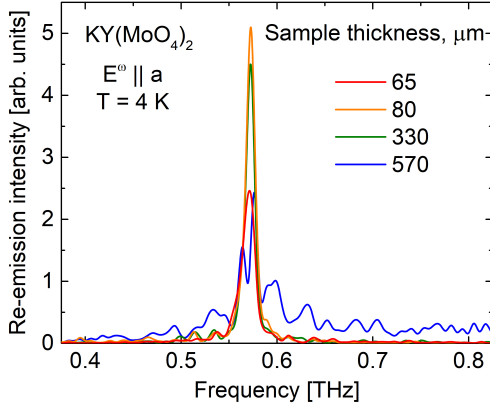


FIG. 5. The thickness evolution of the re-emission spectra of $\text{KY}(\text{MoO}_4)_2$ at 4 K and $E^\omega \parallel a$.

active lattice vibrations as the monochromatic THz radiation [2]. Such coherent phonon re-emission has been reported previously in a different classes of materials ranging from elemental semiconductor tellurium [3] to hybrid perovskites [4] and topological material TaAs [6] but usually on frequencies above 1 THz and in rather broad spectrum. In our experiments, however, exceptionally low energy and long phonons lifetime allows to detect the extremely narrow-band re-emissions with central frequencies of 568 GHz and 860 GHz for $E^\omega \parallel a$ and c crystallographic axes respectively with the decay time of 33 ps. For $E^\omega \parallel a$ we found that the re-emission last for more than 100 ps or more then 50 optical cycles. These unique characteristic together with chemical

durability make $\text{KY}(\text{MoO}_4)_2$ very attractive for variety of THz applications, ranging from a conventional magnetic resonance spectroscopy [24] to narrowband THz pulses generation for novel THz-driven electron acceleration systems [25].

Other materials from the family of $\text{MR}(\text{MoO}_4)_2$ exhibit rather similar phonon spectra below 1 THz. All these compounds have S_a and S_c phonons similar to discussed above with small frequency variation due to different masses of R^{3+} and M^+ ions [14]. Particularly, similar time traces we observed in $\text{KTm}(\text{MoO}_4)_2$ and $\text{KEr}(\text{MoO}_4)_2$ compounds. This create a versatile ground for the development of sub-THz radiation sources. An additional significant advantage is the chemical stability of these materials: they may be kept at the ambient laboratory conditions for decades without changing composition, crystallographic structure and other physical properties. Our experimental results have revealed no difference between samples and obtained in 2024 and in 1980th. $\text{MR}(\text{MoO}_4)_2$ compounds are resistant to standard solvents such as water, acetone, alcohol, which significantly simplify a working protocol.

Acknowledgment

The authors thank N. Stojanovic for useful discussions and suggestions. DK funded by the Deutsche Forschungsgemeinschaft (DFG, German Research Foundation) – 497756533, KV and LP acknowledge funding from the Deutsche Forschungsgemeinschaft (DFG, German Research Foundation) TRR 360-492547816.

-
- [1] D. Mittleman, *Sensing with Terahertz Radiation*, Springer-Verlag Berlin Heidelberg, 2003.
- [2] M. C. Nuss, J. Orenstein, Terahertz time-domain spectroscopy. In: G. Grüner, (eds) *Millimeter and Submillimeter Wave Spectroscopy of Solids*. Topics in Applied Physics, vol 74. Springer, Berlin, Heidelberg, 1998. DOI: <https://doi.org/10.1007/BFb0103419>
- [3] T. Dekorsy, H. Auer, C. Waschke, H. J. Bakker, H. G. Roskos, H. Kurz, V. Wagner and P. Grosse, Emission of submillimeter electromagnetic waves by coherent phonons, *Phys. Rev. Lett.* **74**, 738 (1995). DOI: <https://doi.org/10.1103/PhysRevLett.74.738>
- [4] B. Guzelturk, R. A. Belisle, M. D. Smith, K. Bruening, R. Prasanna, Y. Yuan, V. Gopalan, C. J. Tascone, H. I. Karunadasa, M. D. McGehee, A. M. Lindenberg, Terahertz Emission from Hybrid Perovskites Driven by Ultrafast Charge Separation and Strong Electron-Phonon Coupling, *Adv. Mater.* **30**, 1704737 (2018). DOI: <https://doi.org/10.1002/adma.201704737>
- [5] K. Rabia, F. Meng, M. D. Thomson, M. Bykov, R. Merlin, S. van Smaalen, and H. G. Roskos, Coherent photo-induced phonon emission in the charge-density-wave state of $\text{K}_{0.3}\text{MoO}_3$, *New J. Phys.* **21**, 013013 (2019). DOI: <https://doi.org/10.1088/1367-2630/aaf81f>
- [6] Y. Gao, S. Kaushik, E. J. Philip, *et al.*, Chiral terahertz wave emission from the Weyl semimetal TaAs, *Nat. Commun.* **11**, 720 (2020). DOI: <https://doi.org/10.1038/s41467-020-14463-1>
- [7] N. Kida, T. Miyamoto, and H. Okamoto, Emission of terahertz electromagnetic waves: a new spectroscopic method to investigate physical properties of solids, *J. Phys. Soc. Jpn.* **91**, 112001 (2022). DOI: <https://doi.org/10.7566/JPSJ.91.112001>
- [8] J. P. Guillet, B. Recur, L. Frederique, B. Bousquet, L. Canioni, I. Manek-Hönniger, P. Desbarats, and P. Mounaix, Review of Terahertz Tomography Techniques, *J. Infrared Milli. Terahz. Waves* **35**, 382-411 (2014). DOI: <https://doi.org/10.1007/s10762-014-0057-0>
- [9] E. A. Nanni, W. R. Huang, K.-H. Hong, K. Ravi, A. Fallahi, G. Moriena, R. J. Dwayne Miller, and F. X. Kärtner, Terahertz-driven linear electron acceleration, *Nat. Commun.* **6**, 8486 (2015). DOI: <https://doi.org/10.1038/ncomms9486>
- [10] M. Liu, H. Y. Hwang, H. Tao, A. C. Strikwerda, K. Fan, G. R. Keiser, A. J. Sternbach, K. G. West, S. Kittiwatanakul, J. Lu, S. A. Wolf, F. G. Omenetto, X. Zhang, K. A. Nelson, and R. D. Averitt, Terahertz-field-induced insulator-to-metal transition in vanadium dioxide metamaterial, *Nature* **487**, 345 (2012). DOI: <https://doi.org/10.1038/nature11231>
- [11] C. D. W. Mosley, D. S. Lake, D. M. Graham, S. P. Jamison, R. B. Appleby, G. Burt, and M. T. Hibberd, Large-area periodically-poled lithium niobate wafer stacks optimized for high-energy narrowband terahertz generation, *Opt. Express* **31**, 4041 (2023). DOI: <https://doi.org/10.1364/OE.475604>
- [12] S. Nugraha, G. Krizsán, G. Polónyi, M. I. Mechler, J. Hebling, G. Tóth and J. A. Fülöp, Efficient semiconductor multicycle terahertz pulse source, *J. Phys. B: At. Mol. Opt. Phys.* **51** 094007 (2018). DOI: <https://doi.org/10.1088/1361-6455/aab9ec>
- [13] J. Lu, H. Y. Hwang, X. Li, S.-H. Lee, O.-P. Kwon, and K. A. Nelson, Tunable multi-cycle THz generation in organic crystal HMQ-TMS, *Opt. Express* **23**, 22723 (2015). DOI: <https://doi.org/10.1364/OE.23.022723>
- [14] S. Poperezhai, P. Gogoi, N. Zubenko, K. Kutko, V. I. Kutko, A. S. Kovalev and D. Kamenskyi, Terahertz lattice dynamics of the potassium rare-earth binary molybdates, *J. Phys.: Condens. Matter* **29**, 095402 (2017). DOI: <https://doi.org/10.1088/1361-648X/aa55a8>
- [15] S. Chong, S. Perry, B. J. Riley and Z. J. Nelson, Crystal structures and comparisons of potassium rare-earth molybdates $\text{KRE}(\text{MoO}_4)_2$ ($\text{RE} = \text{Tb}, \text{Dy}, \text{Ho}, \text{Er}, \text{Yb}$, and Lu), *Acta Cryst. E* **76**, 1871-1875 (2020). DOI: <https://doi.org/10.1107/S205698902001542X>
- [16] V. Tkáč, A. Orendáčová, E. Čizmár, M. Orendáč, A. Feher, and A. G. Anders, Giant reversible rotating cryomagnetocaloric effect in $\text{KEr}(\text{MoO}_4)_2$ induced by a crystal-field anisotropy, *Phys. Rev. B* **92**, 024406 (2015). DOI: <https://doi.org/10.1103/PhysRevB.92.024406>
- [17] B. Bernáth, K. Kutko, S. Wiedmann, O. Young, H. Engelkamp, P. C. M. Christianen, S. Poperezhai, L. V. Pourovskii, S. Khmelevskiy, and D. Kamenskyi, Massive magnetostriction of the paramagnetic insulator $\text{KEr}(\text{MoO}_4)_2$ via a single-ion effect, *Adv. Electron. Mater.* **8**, 2100770 (2022). DOI: <https://doi.org/10.1002/aelm.202100770>
- [18] T. Yoshida, K. Nakabayashi, H. Tokoro, M. Yoshikiyo, A. Namai, K. Imoto, K. Chibac and S. Ohkoshi, Extremely low-frequency phonon material and its temperature- and photo-induced switching effects, *Chem. Sci.* **11**, 8989 (2020). DOI: <https://doi.org/10.1039/D0SC02605K>
- [19] A. B. Kuzmenko, Kramers-Kronig constrained variational analysis of optical spectra, *Rev. Sci. Instrum.* **76**, 083108 (2005). DOI: <https://doi.org/10.1063/1.1979470>
- [20] P. F. Lory, S. Pailhes, V. M. Giordano *et al.*, Direct measurement of individual phonon lifetimes in the clathrate compound $\text{Ba}_{7.81}\text{Ge}_{40.67}\text{Au}_{5.33}$, *Nat. Commun.* **8**, 491 (2017). DOI: <https://doi.org/10.1038/s41467-017-00584-7>
- [21] G. Nilsson and G. Nelin, Phonon dispersion relations in Ge at 80 K, *Phys. Rev. B* **3**, 364 (1971). DOI: <https://doi.org/10.1103/PhysRevB.3.364>
- [22] P. K. Jakobsen and M. Mansuripur, On the nature of the Sommerfeld-Brillouin forerunners (or precursors), *Quantum Stud.: Math. Found.* **7**, 315 (2020). DOI: <https://doi.org/10.1007/s40509-019-00210-9>
- [23] Bruno Macke and Bernard Ségard, From Sommerfeld and Brillouin forerunners to optical precursors, *Phys. Rev. A* **87** 043830 (2013). DOI: <https://doi.org/10.1103/PhysRevA.87.043830>
- [24] M. Ozerov, B. Bernáth, D. Kamenskyi *et al.*, A THz spectrometer combining the free electron laser FLARE with 33 T magnetic fields, *Appl. Phys. Lett.* **110**, 094106 (2017). DOI: <https://doi.org/10.1063/1.4977862>
- [25] G. Priebe, D. Laundry, M.A. Macdonald *et al.*, Inverse Compton backscattering source driven by the multi-10 TW laser installed at Daresbury, *Laser and Particle Beams*, **26**(4), 649-660 (2008). DOI: <https://doi.org/10.1017/S0263034608000700>